


ORIGINAL ARTICLE

Aspect ratio of nano/microstructures determines *Staphylococcus aureus* adhesion on PET and titanium surfaces

A.-K. Meinshausen¹, M. Herbster^{1,2} , C. Zwahr³, M. Soldera³, A. Müller^{4,5}, T. Halle², A.F. Lasagni^{3,6} and J. Bertrand¹

1 Department of Orthopedic Surgery, Otto-von-Guericke University Magdeburg, Magdeburg, Germany

2 Institute of Materials and Joining Technology, Otto-von-Guericke University Magdeburg, Magdeburg, Germany

3 Chair of Large Area Laser Based Surface Structuring, Technische Universität Dresden, Dresden, Germany

4 Institute for Molecular and Clinical Immunology, Otto-von-Guericke University Magdeburg, Magdeburg, Germany

5 Helmholtz Centre for Infection Research, Braunschweig, Germany

6 Fraunhofer Institute for Material and Beam Technology IWS, Dresden, Germany

Keywords

aspect ratio, orthopaedic implant, periprosthetic joint infection, *S. aureus*, structures, titanium, PET.

Correspondence

Maria Herbster, Institute of Materials and Joining Technology, Otto-von-Guericke University, Universitätsplatz 2, D-39106 Magdeburg, Germany.
E-mail: maria.herbster@ovgu.de

Ann-Kathrin Meinshausen, Maria Herbster, Andrés Fabián Lasagni and Jessica Bertrand contributed equally to this work.

2021/2282: received 21 October 2020, revised 26 January 2021 and accepted 6 February 2021

doi:10.1111/jam.15033

Abstract

Aims: Joint infections cause premature implant failure. The avoidance of bacterial colonization of implant materials by modification of the material surface is therefore the focus of current research. In this *in vitro* study the complex interaction of periodic structures on PET and titanium surfaces on the adhesion of *Staphylococcus aureus* is analysed.

Methods and Results: Using direct laser interference patterning as well as roll-to-roll hot embossing methods, structured periodic textures of different spatial distance were produced on surfaces and *S. aureus* were cultured for 24 h on these. The amount of adhering bacteria was quantified using fluorescence microscopy and the local adhesion behaviour was investigated using scanning electron microscopy. For PET structures, minimal bacterial adhesion was identified for an aspect ratio of about 0.02. On titanium structures, *S. aureus* adhesion was significantly decreased for profile heights of < 200 nm. Our results show a significantly decreased bacterial adhesion for structures with an aspect ratio range of 0.02 to 0.05.

Conclusions: We show that structuring on surfaces can decrease the amount of *S. aureus* on titanium and PET as common implant materials.

Significance and Impact of the Study: The study highlights the immense potential of applying specific structures to implant materials to prevent implant colonization with pathogen bacteria.

Introduction

Periprosthetic joint infections (PJI) after total joint arthroplasty (TJA) represent a serious complication causing severe suffering, extended hospitalization and challenging revision surgery for the patient. The risk for PJI is about 5.2 % and each revision increases the risk by 10 % to 15 % (Goldberg *et al.* 1988; Fehring 2000; Smucny *et al.* 2015). The worst case of PJI results in a sepsis or the need of an amputation (Goldberg *et al.* 1988; Fehring

et al. 2000; Ulrich *et al.* 2008; Wetters *et al.* 2013; Smucny *et al.* 2015; Sousa *et al.* 2018).

Standard materials used for orthopaedic implants are titanium- or cobalt-base metal alloys, alumina ceramics and polymers. Ultrahigh molecular weight polyethylene (UHMWPE ISO 5834-3:2019) is commonly used as soft bearing component, for the manufacturing of hip inlays for the acetabular cups or as meniscus component in knee implants. UHMWPE exhibits a low density, sufficient impact strength, good biocompatibility and is at the

same time inexpensive and easy to machine (Fisher and Dowson 1991; Sutula *et al.* 1995). Polyester polyethylene terephthalate (PET) fibres are also used for the production of artificial tendon and ligament replacements. The semi-crystalline polymer can fix contracting muscles to bone anchor (Beach *et al.* 1991; Kvist *et al.* 2005). These fibres exhibit an increased hardness, relatively high strength and good stiffness (Gao *et al.* 2010; Melvin *et al.* 2010). Metal alloys, such as pure titanium (ISO 5832-2), titanium-base alloys (ISO 5832-3/-11) or cobalt-base alloys (ISO 5832-4/-12), are used for the manufacturing of load-bearing implant components. Titanium implants are favoured for osseointegration since they ensure an ideal bone apposition on cementless femoral stems or acetabular shells (Gibon *et al.* 2017).

Bacteria are able to colonize all kinds of different implant surfaces in an exogenous or endogenous way (Briandet *et al.* 2001). The risk of developing a PJI is increased in knee (2 %) in contrast with hip arthroplasty (~1 %) (Andrej Trampuz and Werner Zimmerli 2008). Common pathogens causing a PJI are bacteria from the staphylococcal genus, especially *S. aureus* and *S. epidermidis* (Zimmerli and Sendi 2011; Barrett and Atkins 2014; Nair *et al.* 2014). Interestingly, the microbiological spectrum varies depending on the localization of the joint infection (Marculescu and Cantey 2008; Peel *et al.* 2012; Tande and Patel 2014). For example, *Propionibacterium acnes* is found more frequently in shoulder endoprostheses than in other orthopedic implants. (Piper *et al.* 2009). Anaerobic bacteria are more likely to be present in hip PJI than in knee PJI (Marculescu and Cantey 2008). Therefore, different structures might be needed to achieve the bacteria repellent effect for the broad variety of different species with their different shape and size (Jaggessar *et al.* 2017). After the adhesion of the bacteria to the implant material, the bacteria are capable of forming a biofilm (Costerton *et al.* 1999; Webb *et al.* 2003; Hall-Stoodley *et al.* 2004; Høiby *et al.* 2010; Høiby *et al.* 2015). The biofilm formed by bacteria consists of a dense network of polysaccharides, in which extracellular DNA, proteins and bacteria are embedded. The biofilm protects the bacteria from external influences, leading to a higher tolerance towards antibiotics and the immune system (Briandet *et al.* 2001; Flemming and Wingender 2010; Boháčová *et al.* 2019). There are two basic strategies to prevent biofilm formation, either by inhibition of the biofilm formation or by repelling of bacteria from the start. Each patient undergoing a TJA surgery is often pre-operatively treated with a combination of different antibiotics to prevent the perioperative infection (Pavel *et al.* 1974; Pollard *et al.* 1979; Mauerhan *et al.* 1994; Meehan *et al.* 2009). However, this therapy only prevents the immediate infection directly after surgery. Late infections

and haematogenic infections cannot be prevented with this prophylactic therapy (Lentino 2003). Furthermore, the increasing presence of bacterial antibiotic resistance increases the risk for PJI as not all pathogens might be killed with treatment before the surgery (Lentino 2003).

Interestingly, microbial repellency can be achieved by applying a specific surface structure on implant surfaces (Otto 2008; Pavithra and Doble 2008). Various studies investigated the influence of the surface roughness on the adhesion of different bacteria (Esposito *et al.* 2007; Duarte *et al.* 2009; Ivanova *et al.* 2010; Truong *et al.* 2010; Wu *et al.* 2011b). A study showed that holes or craters larger than the bacteria in the surface seem to inhibit the formation of bacteria colonies (Epperlein *et al.* 2017; Zwahr *et al.* 2019a). Since colony clustering is an essential precondition for the formation of a biofilm, these structures might inhibit biofilm formation. It is known that rough surfaces in the macro and micro scale, however, increase microbial adhesion. In particular, surface profiles in the size of the bacteria (about 1 μm) provide maximum contact area and thereby enhance adhesion. Slightly smaller structure patterns within the micrometer and submicron range decrease the bacterial adhesion (Medilanski *et al.* 2002; Whitehead *et al.* 2005; Helbig *et al.* 2016; Epperlein *et al.* 2017; Lutey *et al.* 2018; Zwahr *et al.* 2019a). In this context, recent studies investigated bacterial adhesion on nanorough titanium surfaces by applying different deposition techniques (Jaggessar *et al.* 2017), including magnetron sputtering (Whitehead *et al.* 2005; Ivanova *et al.* 2010) physical vapour deposition (Lüdecke *et al.* 2013), supersonic cluster beam deposition (Singh *et al.* 2013) or laser-based structuring techniques (Cunha *et al.* 2016; Helbig *et al.* 2016; Rosenkranz *et al.* 2016; Epperlein *et al.* 2017; Lutey *et al.* 2018; Schwibbert *et al.* 2019; Florian *et al.* 2020; Jalil *et al.* 2020). These studies proved a significant reduction in bacterial adhesion at a mean roughness of 2 to 20 nm. However, the different structuring techniques vary in their uniformity and generate different surface properties regarding porosity, chemical composition (e.g. metal oxides, chemical residues) and surface energy. Since these characteristics influence bacterial adhesion in combination with surface topography, a comparison of results from different techniques is difficult. In addition, the specific geometric parameters including the spatial and vertical surface parameters cannot be applied in a reproducible manner.

Direct laser interference patterning (DLIP) is a fast and cost-efficient processing technology to generate high-resolution structured surface features of different morphology. For example, using two laser beams which are overlapped under a certain angle, it is possible to generate an interference pattern with a line-like periodic intensity distribution (Lasagni *et al.* 2009; Rodriguez *et al.* 2009; Bremus-Koebberling *et al.* 2012; Oliveira *et al.*

2012; Zwahr *et al.* 2019a). Later, based on photothermal or photochemical interaction of the laser light with the material, wave-like patterns of high homogeneity are formed since the material surface is locally ablated or modified at the interference maxima positions. Furthermore, the DLIP method can be used for treating large-area hot-embossing tools, which permit to transfer the surface topography of the metallic tools to polymer foils at processing speeds of several square meters per minute (Soldara *et al.* 2020).

The present study investigates the potential of DLIP generated structures for inhibition of bacterial adhesion. Therefore, the resulting morphology and roughness of directly treated titanium (Ti) surfaces as well as indirectly processed polyethylene terephthalate (PET) foils using roll-to-roll (R2R) hot-embossing is analysed with confocal microscopy. The adhesion of *S. aureus* on the different structures in comparison to polished reference surfaces is evaluated. Scanning electron microscopy is applied to visualize the bacterial adhesion. The aim is to identify critical structuring parameters that exhibit the best *S. aureus* repellence.

Materials and methods

Sample fabrication

Direct laser interference patterning (DLIP) was applied to generate structures on commercially pure titanium discs (Ti grade 4 ISO 5832-2) with 25 mm in diameter. By varying the angle between the two interfering laser beams, the distribution of the interference intensity was modified and different spatial periods of the periodic wave-like structures were generated. In addition, the profile height was customized by adjusting the processing speed and laser energy density, also known as laser fluence. A brief description of the DLIP method with schematic illustration is included as supplementary information (Fig. A1(a)). In total, five structures were generated with different spatial periods ranging from 700 nm to 5 μm and profile heights of 100 nm to 800 nm as summarized in Table 1. As reference, a polished Ti-6% Al-4%V wrought alloy sample (ISO 5832-3) with a diameter of 13 mm was used. Further information about this method has been published elsewhere (Voisiat *et al.* 2019).

For processing the PET foils, the following approach was used. First, nickel sleeves with a thickness of 200 μm , 300 mm wide and with a diameter of 300 mm (Saechsische Walzengravur GmbH, Frankenberg, Germany) were used for DLIP structuring. The initial surface roughness S_a was 61 nm. Prior to the laser process, the sleeves were cleaned from contaminations using ethanol.

Table 1 Processing and geometric parameters of the line-like structured Ti samples using DLIP

Ti sample ID	Fluence (J cm^{-2})	Spatial period (μm)	Profile height (nm)
A	0.9	~ 5	~ 800
B	0.29	~ 2.2	~ 500
C	0.06	~ 1.3	~ 200
D	0.06	~ 0.7	~ 180
E	0.47	No periodicity, random structures	~ 100
Control	No	No	~ 200

Next, the nickel sleeves were processed using a 3D-DLIP unit employing a rotary axis system (developed at the TU-Dresden, Germany). The 3D-DLIP structuring system utilizes a solid-state ps-laser with 1064 nm laser wavelength (Edgewave PX200, Germany) and a pulse duration of 10 ps. Line-like structures with a spatial periods of 4.3 μm , 3.8 μm , 2.5 μm and 1.5 μm were produced. The spot diameter was 190 μm and the employed single pulse laser fluence was 0.36 J cm^{-2} for all spatial periods. By changing the pulse to pulse overlap, the depth of the periodic structures was varied. The cumulated used fluence (resulting from the different pulse to pulse overlaps) for processing the Ni-sleeve is listed in Table 2. Finally, the PET film samples were processed using the DLIP treated Ni-sleeve in a roll-to-roll (R2R) hot-embossing system (R2R Basecoater BC51, Coatema Coating Machinery GmbH, Germany) at an embossing

Table 2 Processing and geometric parameters of the line-like structured PET samples

PET sample ID	Used cumulated fluence for Ni-sleeve (J cm^{-2})	R2R web speed (m min^{-1})	Spatial period (μm)	Profile height (nm)
1	7.2	2	4.3	~ 400
2	3.6	2		~ 100
3	1.8	2		< 50
4	7.2	2	3.8	~ 500
5	3.6	2		~ 200
6	1.8	2		~ 100
7	7.2	12	2.5	~ 600
8	7.2	4		~ 550
9	7.2	1		~ 400
10	7.2	2		~ 400
11	3.6	2		~ 250
12	1.8	2		~ 100
13	7.2	2	1.5	~ 400
14	3.6	2		~ 250
15	1.8	2		~ 200
Control	No	No	No	~ 100

temperature of approximately 90°C and at varying web speeds between 1 m min⁻¹ and 12 m min⁻¹ (Rank *et al.* 2017). The R2R method is illustrated schematically in the supplementary Fig. A1(b).

Four different spatial period groups were produced in this case. For each periodic group different profile heights were obtained by either varying the pulse to pulse overlap during the fabrication of the Ni-sleeve or by changing web speed in the R2R process, as listed in Table 2. A total of 15 samples with structure heights in the range of 30 nm to 600 nm were generated and tested (Table 2). The PET reference was the untreated source material. Each specimen was customized cut to a size of 8 × 8 mm².

Surface morphologies and roughness

3D topographic images were obtained with a confocal microscope (μ surf expert, NanoFocus AG, Oberhausen, Germany). The measuring field of 163 × 163 μ m² was acquired with a 100× magnification objective and a vertical resolution of 1 nm. All samples were measured at three different locations. Roughness parameters, including the arithmetic average roughness (R_a), the average maximum profile height (R_z), the core groove depth (R_k DIN EN ISO 13565-2) and mean line spacing of roughness peaks (RSm), were determined according to the standard ISO 4287. Representative 3D surface images and 2D roughness profiles were obtained on an extracted area of 20 × 20 μ m².

Bacterial adhesion test

To test the bacterial adhesion of the structured PET and Ti surfaces, the samples were incubated three times with *S. aureus* SH1000 pSB2035 (Qazi *et al.* 2001). This *S. aureus* strain constitutively expresses the green fluorescent protein (GFP). *S. aureus* was cultured overnight in tryptic Soy Broth (TSB). The structured test plates were incubated with 1 ml TSB media and inoculated with a 1:1000 dilution of the *S. aureus* overnight culture that was adjusted to an optical density (OD_{600 nm}) of 1 for 24 h at 37°C. To prevent contamination, we inoculated the overnight culture from our glycerol stock solution and worked under standard sterile conditions. The metal disks were sterilized using heat inactivation. The medium was removed and the PET and Ti plates were washed twice with phosphate buffered saline (PBS) and subsequently fixed with 4 % paraformaldehyde for 30 min at room temperature. The amount of adhering bacteria was quantified in 630× magnification microscopic pictures (Zeiss fluorescence microscope Axio Observer.Z1, Jena, Germany). The fluorescence of the GFP was excited by a

wavelength of 488 nm and a read out of 500 – 550 nm. Pictures from five different randomly chosen, representative areas from each sample were taken and evaluated by counting the amount of bacteria with ImageJ software. In ImageJ we set a threshold to reduce the background fluorescence and to measure only the intensity of the GFP fluorescence (Bui *et al.* 2020).

Cleaning and sterilization of the samples

Before *in vitro* incubation, all PET samples were cleaned in pure isopropanol and dried under sterile conditions. Afterwards they were placed under UV light for 24 h. The Ti specimens were cleaned by incubating them for 30 min in 10 ml of RIPA Buffer (150 mmol l⁻¹ sodium chlorid, 1.0 % Triton X, 0.5 % sodium deoxycholate, 0.1 % SDS, 50 mmol l⁻¹ Tris) at room temperature. RIPA is a lysis buffer used for cell lysis and protein solubilization. This reagent is capable of extracting cytoplasmic, nuclear and membrane proteins. Afterwards the platelets were incubated with Trypsin for 30 min at 37°C under sonification. The Ti specimens were rinsed with distilled water and incubated in 70 % ethanol. For sterilization, the Ti plates were flamed for sterilization and placed under UV light for 24 h. Applying this cleaning procedure, the Ti specimens were reused three times. After cleaning, all plates were checked for residual fluorescence indicating adhering bacteria by microscopy. No evidence of GFP fluorescence was observed on the Ti surfaces after the extensive cleaning process using RIPA buffer and trypsin under sonication to remove remaining proteins and adhering bacteria. The PET surfaces were not reused, but new samples were used for each experiment.

Scanning Electron Microscopy analysis

Before or after incubation with *S. aureus*, all PET and Ti surfaces were analysed using scanning electron microscopy (SEM, FEI Scios DualBeam, Thermo Fisher Scientific, Waltham, USA). SEM investigations were conducted using an acceleration voltage of 10 – 15 keV. Regions of interest were identified using an imaging mode at lower magnifications (2000×). Surfaces were imaged with a secondary electrons (SE) detector.

Statistical analysis

If not stated otherwise, the data are presented as mean ± standard deviation (SD). The Friedman test was applied to test for statistical significance. The level of significance was set at $P < 0.05$ for all statistical tests. Statistical analysis was performed using GraphPad Prism (ver. 7, GraphPad Software, San Diego, USA) and Origin

software 2018 (OriginLab Corporation, Northampton, USA). The graphs presented in this study show the mean values with standard error of mean (SEM).

Results

Characterization of structures

Different periodic profile distances with varying profile heights were generated by DLIP and R2R hot-embossing. Figure 1 shows representative 3D confocal microscopic images of the investigated PET and Ti surfaces. In general, the surfaces exhibit a high regularity and homogeneity of the line-like structures. The shapes of all structures

are similar and independent of the decrease of surface roughness. We detected only few surface defects on Ti samples that exhibit spatial periods smaller than $1\ \mu\text{m}$. These defects deteriorate the periodicity of the structures leading to a reduced homogeneity (Fig. 1c,d lower row). Superimposed on the DLIP microstructures, smaller quasi-periodic features were also visible on both the Ti and PET samples that could be identified as the so-called laser-induced periodic surface structures (LIPSS). Figure A2 of the supplementary information shows exemplary SEM images of structured (a) Ti and (b) PET indicating the polarization of the laser beams relative to the grooves' alignment. In both Ti and PET micrographs, low spatial frequency LIPSS (LSFL) and high spatial

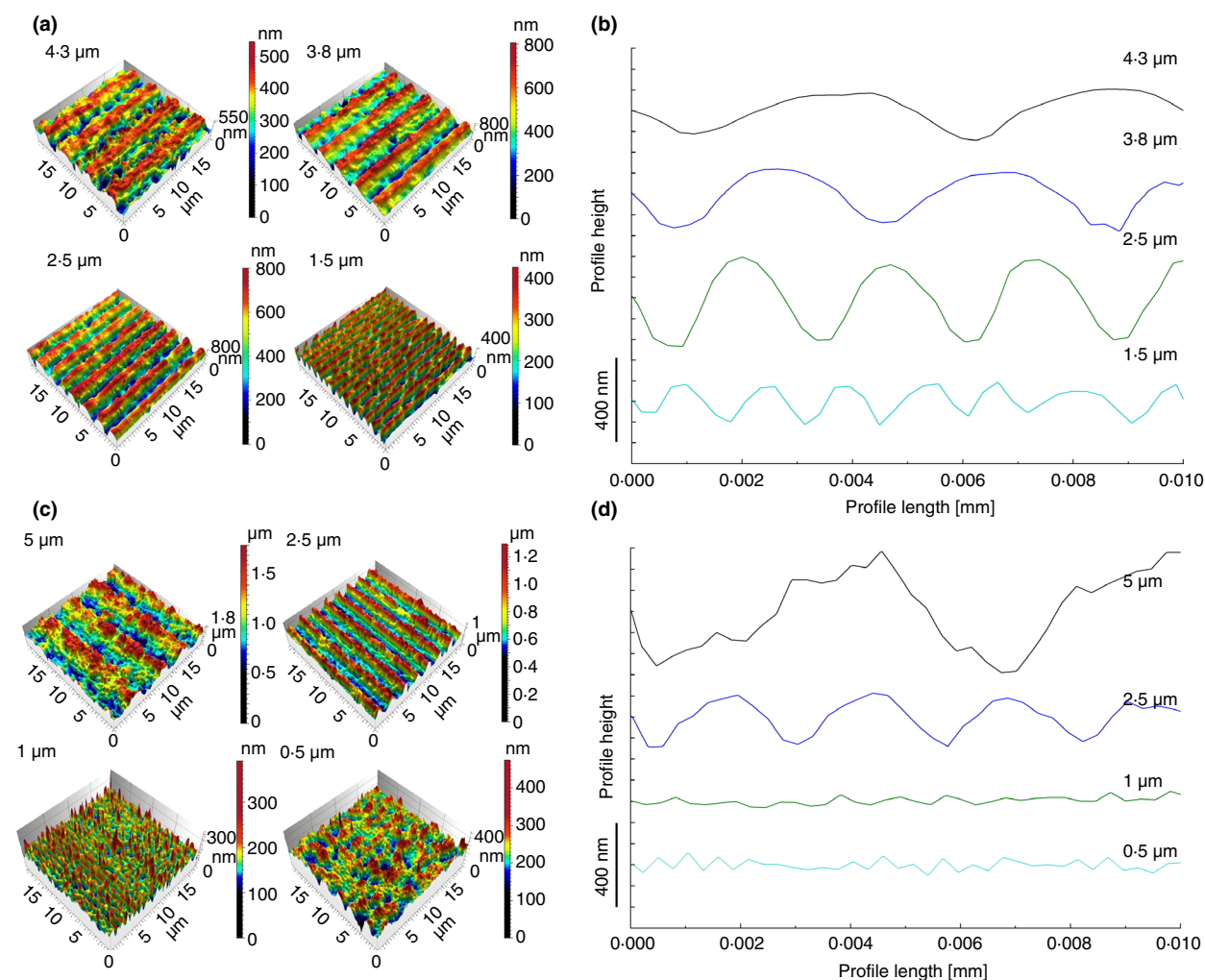


Figure 1 Morphological investigation of the tested samples with different structures. (a) 3D confocal microscopic images of the PET samples of varying heights and spatial periods of 4.3 μm , 3.8 μm , 2.5 μm and 1.5 μm . (b) Roughness profiles over a length of 20 μm perpendicular to the line structures of the investigated PET surfaces. (c) Exemplary images of the Ti samples showing different linear profile heights and spatial periods of 5 μm , 2.5 μm , 1 μm and 0.5 μm . (d) Roughness profiles of the investigated Ti samples.

frequency LIPSS (HSFL) are indicated. It is worth to notice that the LIPSS observed on the PET surface, were produced originally on the Ni sleeve and transferred to the polymer during the hot embossing process. In both materials the LSFL were aligned perpendicular to the radiation polarization and had a spatial period of approximately 800 nm, which is ~ 80 % of the used wavelength. These characteristics are in agreement with previous works on laser irradiation on metals with ultra-short pulses in the near-infrared spectrum (Römer *et al.* 2009; Vincenc Obona *et al.* 2011). It is commonly accepted that LSFL are produced by the interaction of the laser radiation with an electromagnetic wave scattered at the rough surface of strongly absorbing materials, such as metals, involving the excitation of surface plasmon polaritons (Bonse *et al.* 2017). In turn, the HSFL indicated in the

SEM images of the supplementary Figure A2 presented a spatial period of approximately 150 nm and were aligned parallel to the polarization. Although the origin of the HSFL is still under debate, several studies confirm the presence of such nanostructures on Ti and Ni upon irradiating the surfaces with ultra-short pulses as observed in our work (Wu *et al.* 2011a; Höhm *et al.* 2015; Lang *et al.* 2017; Zwahr *et al.* 2019b).

The determined roughness parameters are summarized in Fig. 2. The mean values of the mean line spacing of profile peaks (RSm) vary in the range of 1.46 μm to 5.1 μm for PET samples and between 0.69 μm to 5.18 μm for Ti surfaces (Fig. 2a). Based on the profile distances, four PET gradation groups were generated with mean values of 4.3 μm (sample number: 1–3), 3.8 μm (4–6), 2.5 μm (7–12) and 1.5 μm (13–15). The

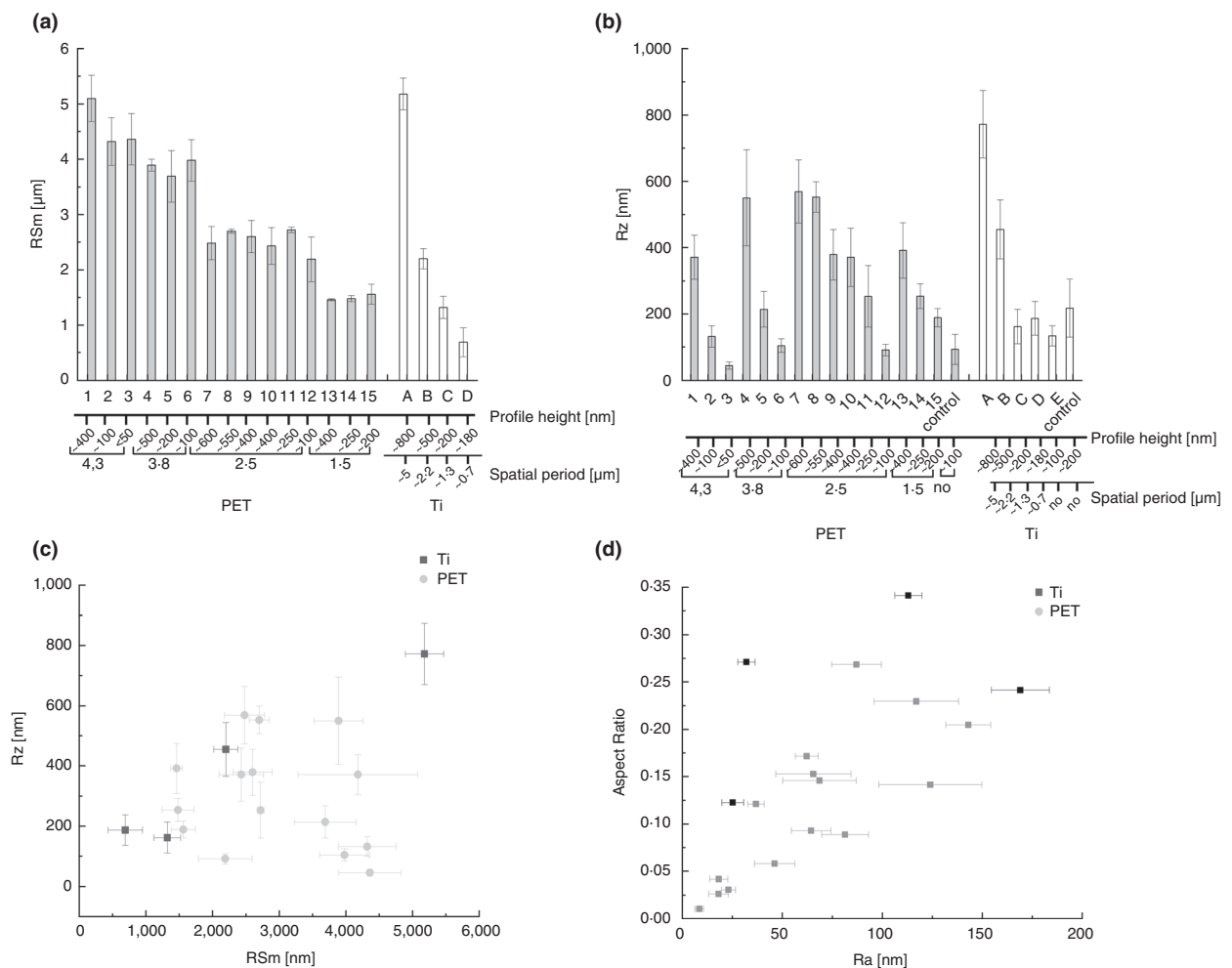


Figure 2 Results of the confocal roughness measurements. (a) Mean values \pm SD of the mean line spacing of profile peaks (RSm) that represent the spatial distances of structures on the PET and Ti samples. (b) Mean values of the average maximum profile height (R_z) of the PET and Ti structures. (c) Correlation of the mean R_z and RSm values of the PET and Ti structures. (d) The arithmetic mean roughness R_a of the structured surfaces and the corresponding aspect ratio (R_z/R_{Sm}) of the produced samples. (■) Ti and (●) PET.

corresponding mean values of the average profile heights (R_z) reveal variations in the size range of 45 nm to 550 nm for the PET specimen. The aspect ratio is defined in this work as the ratio between R_z and RSm (Fig. 2c). Accordingly, each periodic PET group exhibit different aspect ratios, as illustrated in Fig. 2d. The corresponding mean values of the arithmetic mean roughness (R_a) varied between 4 nm to 143 nm for the PET specimens. The Ti samples exhibit mean values of R_z in the range of 162 nm to 772 nm with corresponding R_a values between 25 nm and 162 nm. The reference sample of polished TiAl6V4 alloy exhibits the lowest mean R_a value of 9.6 ± 2 nm. Figure 2d demonstrates the sample roughness distribution according to the arithmetic mean roughness value (R_a) and the corresponding aspect ratio. The mean R_a values range between 8 nm to 170 nm with different aspect ratios (range 0.01 to 0.35).

Influence of structures on bacterial adhesion on PET and Ti surfaces

The *in vitro* quantification of *S. aureus* adhesion to the structured PET surfaces is shown and summarized in Fig. 3. An unstructured PET surface was used as control surface (mean value of adherent bacteria 2512.0 ± 423 on an area of $283.48 \mu\text{m} \times 179.54 \mu\text{m}$). The amount of bacteria adhering to the surfaces did differ significantly depending on the roughness height and the spatial distance of the sample. The sample 2 (1146 ± 273 $P = 0.0038$), sample 6 (1131 ± 958 $P = 0.0175$) and sample 11 (1065 ± 668 $P = 0.0411$) showed significantly less adherent bacteria compared to the control group. In contrast, we observed higher number of bacteria compared to the control group in sample 4 (2586 ± 760) with a spatial distance of $3.8 \mu\text{m}$. Also the samples 7 (2234 ± 1579) and sample 8 (2234 ± 745) with a spatial period of $2.5 \mu\text{m}$ as well as sample 14 (2391 ± 1775) with lowest spatial period of $1.5 \mu\text{m}$ seemed to increase the number of bacteria adhering. A selection of representative microscopic pictures is given in Fig. 3b. As the *S. aureus* strain produced GFP the green area represents the amount of adhering bacteria.

The location of *S. aureus* attaching to the structured PET samples was further investigated using SEM. Representative electron micrographs of bacteria adhering to structures with a spatial periods in the range of $2.5 \mu\text{m}$ are shown in Fig. 4. We observed different bacteria adhesion patterns with decreasing profile heights. Roughness profile heights of about 550 nm, representing half of the bacteria size, lead to a linear orientation of single or coupled bacteria along the parallel profile grooves (Fig. 4a). In contrast, a structure with decreased profile height in the range of 400 nm (Fig. 4b) exhibited an increased

amount of bacteria within the profile grooves of the structure. Clusters of at least four bacteria accumulated inside the grooves. These bacterial accumulations were present within all grooves, covering several machining lines. In the texture with a profile height of about 250 nm only few single bacteria adhered to the surface. The present bacteria did only vaguely correlate with the groove patterning. Furthermore, they appear to adhere only with limited superficial contact without close contact to each other (Fig. 4c). These results are in line with the quantification data.

The results of adhering *S. aureus* on structured Ti surfaces are shown in Fig. 5. The quantification of adherent bacteria is given in Fig. 5a. As control surface (4135 ± 98 bacteria), a polished TiAl6V4 wrought alloy ($R_a = 9.6 \pm 2.1$ nm) sample was used. In comparison to the unstructured control sample all structured surfaces show a significant reduction in the number of adhering bacteria. We found that with decreasing profile height from $1.5 \mu\text{m}$ (sample A) to 180 nm (sample D) the number of bacteria was decreased more efficiently. At the lowest profile height (1648 ± 140 bacteria; $P = 0.0376$) the strongest reduction was observed. However, no significant differences were measured between the different applied structures (A–E). Fig. 5b shows representative microscopic images that were used for the quantification of the bacteria on the tested structured samples. *S. aureus* bacteria are depicted as green fluorescence.

In order to visualize the localization of *S. aureus* on the different structured Ti surfaces, SEM was applied. At a magnification of $6500\times$, the linear structures on the Ti surface are present as parallel filament-like structures that vary in thickness and length with few minor defects and pores (Fig. 6, upper row). At higher magnification ($20\,000\times$) *S. aureus* bacteria can be seen roundly shaped and adhering in grape-like clusters. Interestingly, fewer clusters are observed with a decreased profile height (Fig. 6b,c). These results are in line with the quantification data.

Discussion

The aim of this study was to investigate the effect of periodic structures of wave-shaped morphology with varying surface nanoroughness on the adhesion of *S. aureus*. All structured samples were compared with clinical relevant control surfaces regarding the short-term adhesion of *S. aureus*.

Different repellency strategies for medical implants can be applied in order to generate antibacterial properties either by film deposition, smoothing or roughening of the machined surfaces (Esposito *et al.* 2007; Jaggessar *et al.* 2017). All surface modifications are supposed to

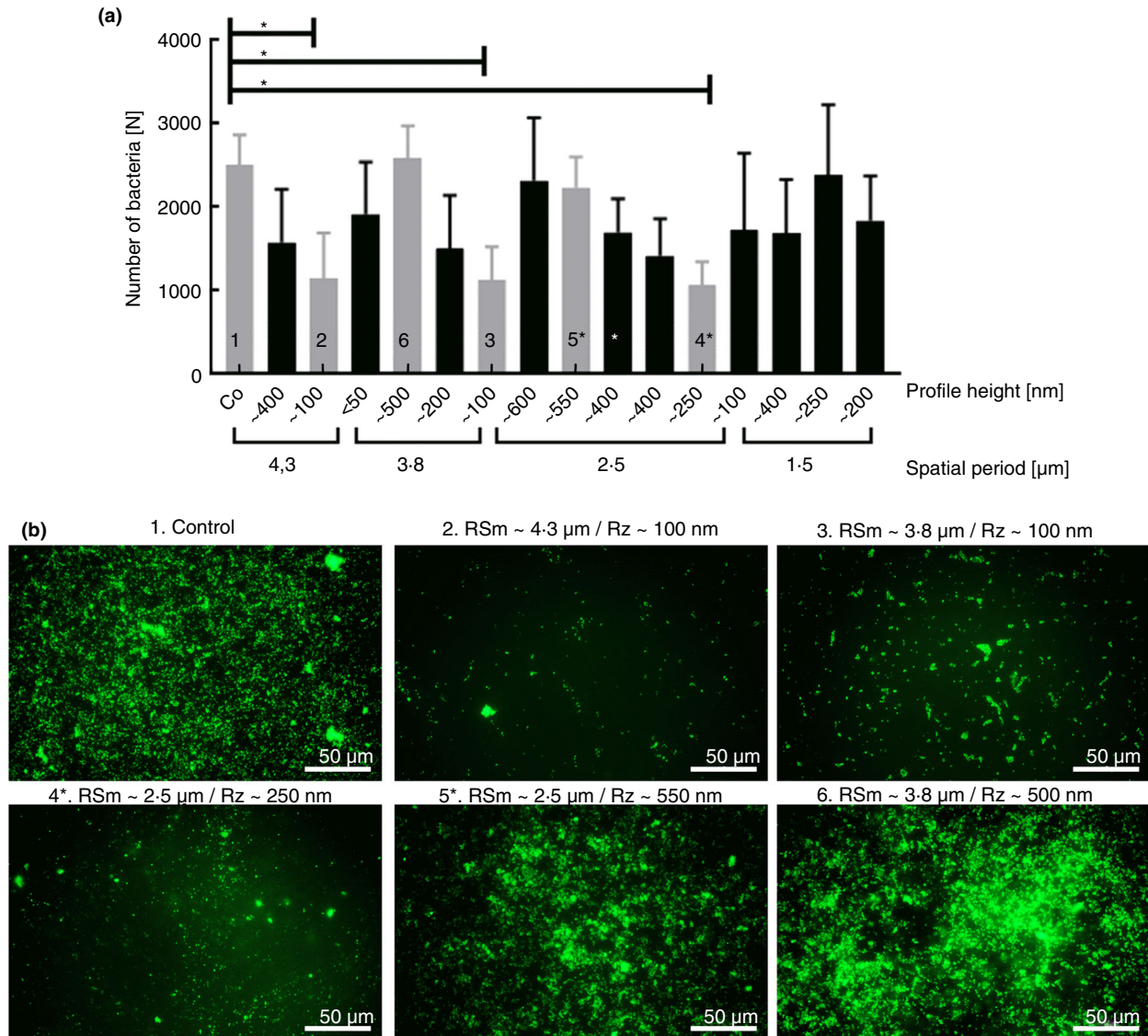


Figure 3 *In vitro* testing of antibacterial properties of structured PET surfaces. (a) Quantitative analysis of the number of *Staphylococcus aureus* on the PET surfaces. The bacteria were incubated on the surfaces for 24 h and then fixed for microscopy, representative areas ($n = 4$) were microscopied and the number of bacteria were analysed via ImageJ Tool. The diagram shows the mean values with SEM. The fluorescence images of the bars marked in light grey can be seen in b, the numbering of the bar charts from 1 to 6 indicates the order of the fluorescence figures in b. The surfaces marked with an asterisk were subsequently examined with SEM (Fig. 4). (b) The fluorescence microscopy images were taken at a magnification of $630\times$. The scale bars (white bars) are $50\ \mu\text{m}$. $*P < 0.05$; n , total number of measurements, N , number of bacteria.

hinder the adhesion of bacteria to the implant surface and inhibit the formation of a biofilm (Hasan *et al.* 2013). Besides biochemically modified surfaces, there is also the possibility of surface structuring. Previous studies have already shown that the surface roughness has an influence on the adhesion of micro-organisms (Esposito *et al.* 2007; Duarte *et al.* 2009). Rougher surfaces tend to increase the microbial adhesion due to a greater surface area, mechanical provision of protection and the presence

of grooves and pits, which influence positively the shear forces of the pathogens (Nyvad and Fejerskov 1987; Morgan and Wilson 2001). Different techniques exist to apply desired structures to implant surfaces. However, low process costs, high pattern resolution and complexity for nanoscale features are the current technological challenges (Lunelli *et al.* 2012). The present study applied DLIP and R2R hot-embossing methods to generate periodic structures on PET and Ti samples. The characterization of the

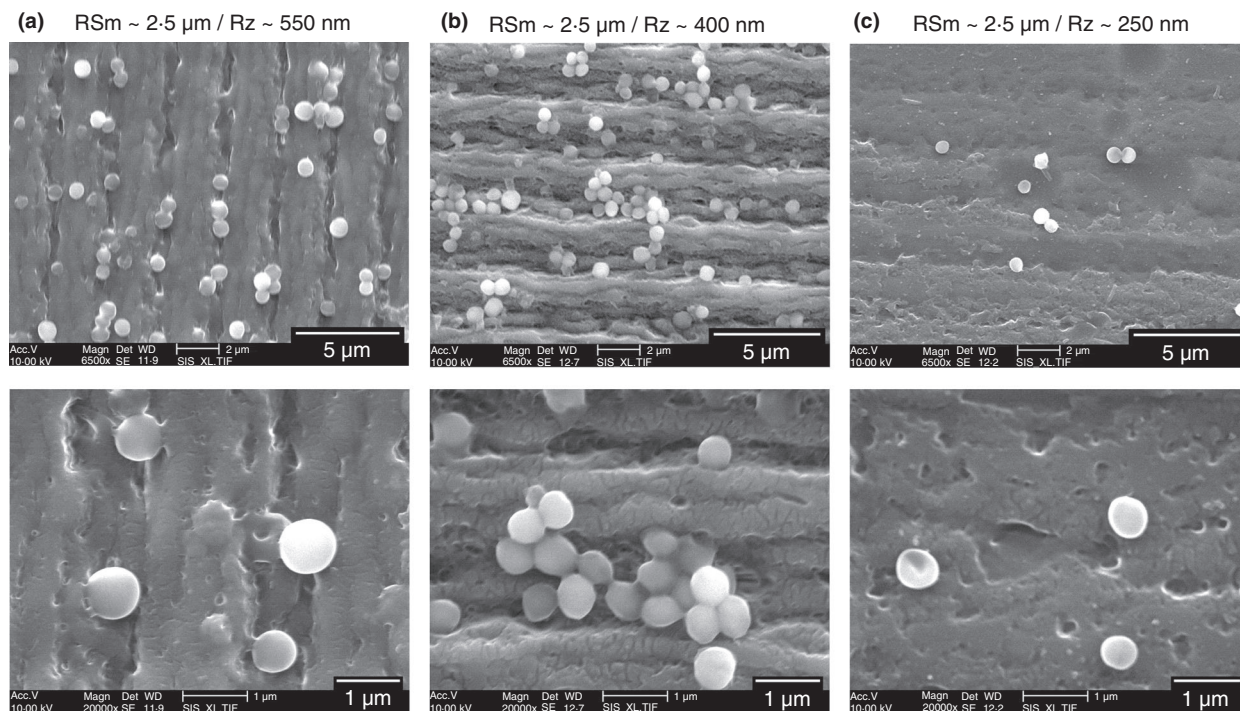


Figure 4 Electron micrographs showing the location of *Staphylococcus aureus* on structured PET samples of a similar spatial distance (RSm of 2.5 μm) with different height profiles (R_z range of 550 nm to 250 nm). Different localization spots of bacteria on the structures were observed (SEM magnification top: 6500 \times , down: 20 000 \times). (a) Coupling of *S. aureus* and linear orientation within the profile grooves. (b) Grouping of several bacteria in the roughness depths and connecting over profile peaks. (c) Single bacteria that adhere irregularly to the shallow structures.

produced structures demonstrated a high homogeneity, consistency and reproducibility of the wave-like profiles for all tested profile heights on PET. In contrast, the Ti samples exhibited variable filament-like structural surfaces with inhomogeneities being present in structures with spatial distances smaller than 1 μm (Figs 1 and 6). These differences in the applied structure contour can be attributed to the laser treatment that transfers energy to the material surface. In particular, it is known that when using ps-laser sources, LIPSS can be formed which cover the surface of the periodic DLIP structures (Fu *et al.* 2019). Additionally, during this process the increasing temperatures melt the surface of the titanium bulk material, change the surface constitution and induce the formation of thicker oxide layers that is accompanied by microporosity. The DLIP generated thin reactive layers on Ti have been previously investigated by Zwahr *et al.* (2019a). Cunha *et al.* (2016) studied the effects of surface characteristic of laser structured Ti surfaces on the adhesion of bacteria. The study verified that the chemical composition of the oxide layer and surface wettability have a minor effect on *S. aureus* adhesion in contrast to surface topography that was also confirmed by Helbig *et al.* (2016). Further research regarding the DLIP processing parameters is required in order to increase the

structural resolution of the Ti structures with minimal spatial distance of smaller than 1 μm .

The profile heights of the different patterns vary between 30 nm to 600 nm for PET and 100 nm to 800 nm for Ti and result in mean R_a values of 4 nm to 143 nm and 25 nm to 162 nm for PET and Ti, respectively. This range of applied nanoroughness was chosen because previous studies found the lowest bacterial adhesion in this range (Whitehead *et al.* 2005; Ulrich *et al.* 2008; Sousa *et al.* 2018). In combination with varying spatial distances of the wave-like shapes, the structures cover an aspect ratio range from 0.01 to 0.35. The *in vitro* testing results revealed that the vertical and horizontal feature size of the structures influenced the amount and location of adhering bacteria. Based on the results of quantitative *in vitro* tests, *S. aureus* adhesion correlated with the aspect ratio of the structures and exhibited a maximum threshold at 0.15. As shown in Fig. 7, minimal bacterial adhesion is present for an aspect ratio in the range from 0.02 to 0.05 followed by few bacterial contacts between 0.05 and 0.12 in comparison to the control. We did not observe a marked difference between Ti and PET structured samples. Nevertheless, a further decrease in aspect ratio (<0.01), similar to surface smoothening, results in an increased microbial adhesion.

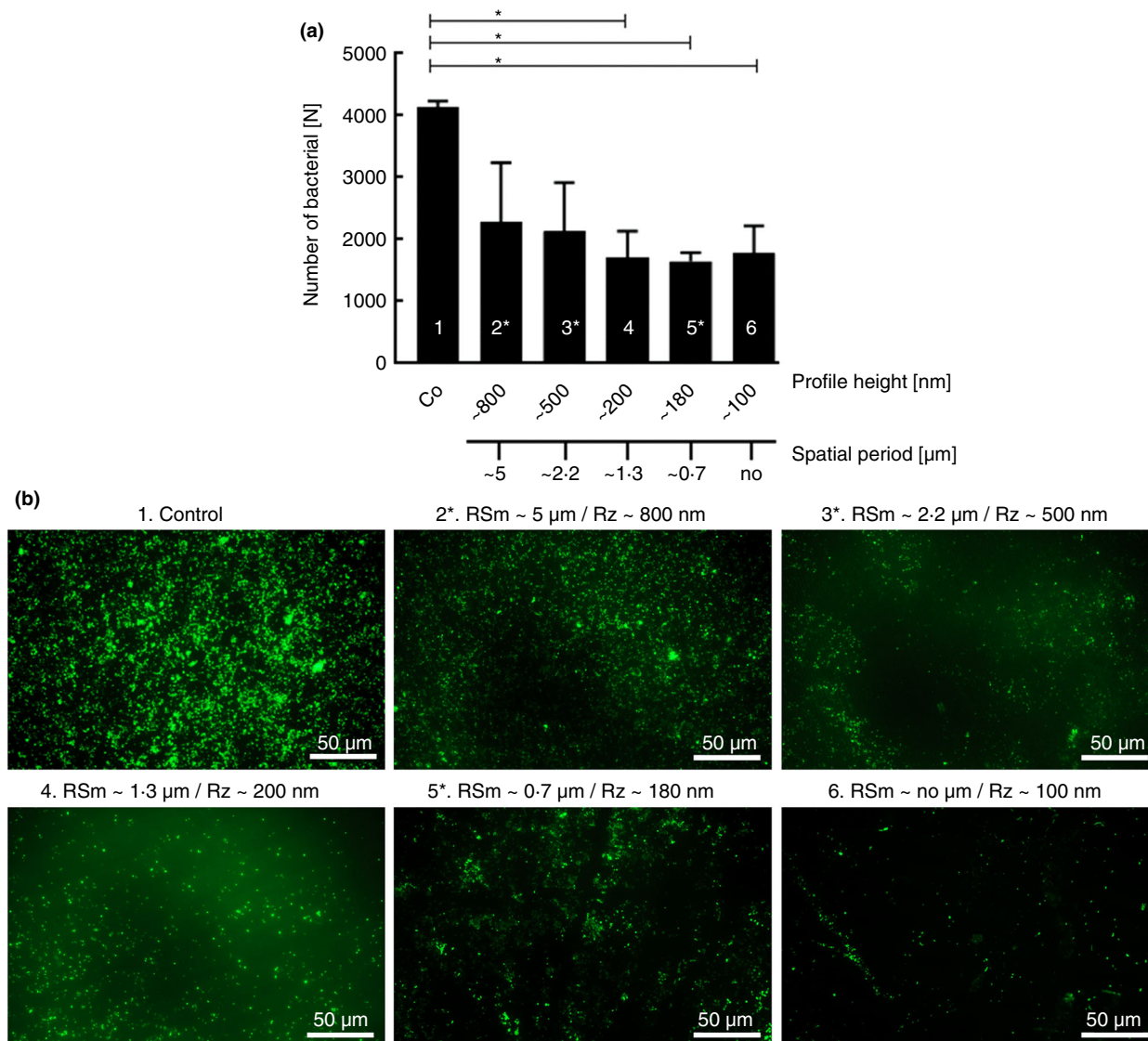


Figure 5 *In vitro* testing of antibacterial properties of structured Ti surfaces. (a) Quantitative analysis of the number of *Staphylococcus aureus* on the Ti surfaces. The bacteria were incubated on the surfaces for 24 h and then fixed for microscopy, representative areas ($n = 4$) were microscopied and the number of bacteria were analysed via ImageJ Tool. Shown is the mean with SEM. The numbering of the bar charts from 1 to 6 indicates the order of the fluorescence figures in b. The surfaces marked with an asterisk were subsequently examined with SEM (Fig. 6) (b) The fluorescence microscopy images were taken at a magnification of 630 \times . The scale bars (white bars) are 50 μm . * $P < 0.05$; n , total number of measurements, N , number of bacteria.

Different publications verified an increased bacterial adhesion on titanium for a roughness range of R_a between 1 nm to 4 nm which corresponds to polished surfaces (Ivanova *et al.* 2010; Truong *et al.* 2010; Wu *et al.* 2011b). This effect is supported by the fact that very smooth surfaces promote an increased production of extracellular polymeric substances (EPS) which are essential for the biofilm formation (Whitehead and Verran 2007). Interestingly, an aspect ratio of 0.15 shows a similar increased adhesive susceptibility compared to the

smooth reference samples. The structures with an aspect ratio of 0.15 cover a wide R_a range of 50 nm to 150 nm, but the results highlight that this characteristic ratio between nanometer sized feature to the spatial period in combination with the superimposed LIPSS enables an ideal surface contact of *S. aureus* as well as an increased bacteria agglomeration within the forming recesses. The resulting cell-surface interaction promotes the aggregate formation of *S. aureus* as prerequisite for colonization (Fig. 7a). An aspect ratio that exceeds 0.2 results in a

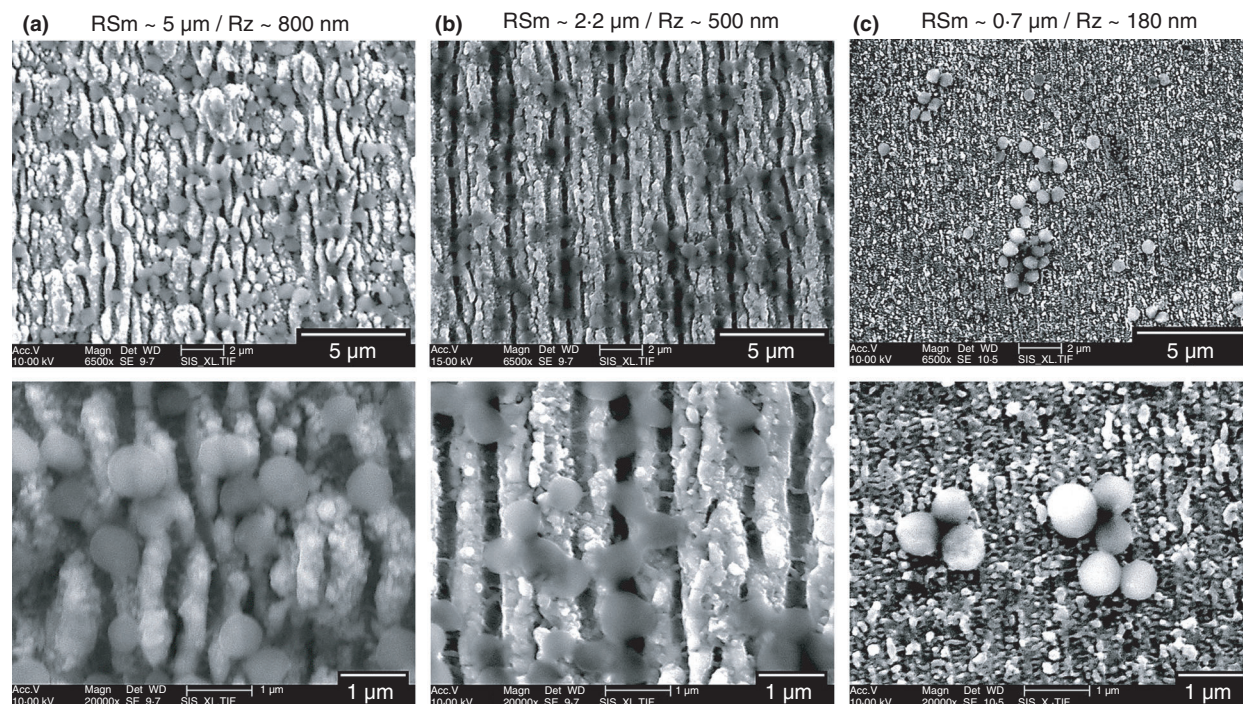


Figure 6 Representative electron micrographs of the location of adhering *Staphylococcus aureus* on the structured Ti surfaces. Along and within the porous linear profile lines, different bacterial clusters are observed (SEM magnification top: 6500 \times , bottom: 20 000 \times). (a) Multiple bacteria clusters cover the structured surface. The bacteria are arranged along the parallel filament lines. (b) Structure with a spatial distance pattern of 2.2 μm shows adhering bacteria clusters. (c) Ti surface with very fine structures in the height of 180 nm show very few bacteria clusters.

reduction of adhering *S. aureus*. Comparable adhesive behaviour was observed for *S. aureus* strains on PET as well as on Ti surfaces. The aspect ratio influences the attachment contact area between microorganism and material and consequently the adhesion and colonization behaviour (Singh *et al.* 2011). A minimal contact area of the bacterium with the surface reduces the interaction energy and results in single or coupled bacteria that adhere to the surface (Bhushan *et al.* 2009; Guo *et al.* 2011; Renner and Weibel 2011). While smooth surfaces provide an ideal large contact area for adhering bacteria, our results highlight that surface profiles with characteristic dense features of nanometer height, smaller than the bacterium size, reduce the contact area for *S. aureus* due to inhibited penetration of the bacteria into the recesses of the structures. The limited attachment of the bacteria to individual surface features decreases the total contact area and thus reduces the adhesion strength of the individual bacterium to the material in contrast with the polished reference samples. This inhibitory adhesion was also demonstrated by Cunha *et al.* (2016) who observed a reduction in *S. aureus* adhesion on femtosecond titanium LIPSS and nanopillars in contrast to polished titanium samples. Similar antimicrobial effects of LIPSS and nanopillars on stainless steel were also demonstrated by

Lutey *et al.* (2018) for *E. coli* and *S. aureus*. These identified effects can explain the significant reduction of adhering bacteria in the aspect ratio range of 0.02 to 0.12 on our samples.

Based on current publications, the *size and shape of the bacteria* play an important role during the colonization of different material surfaces. Epperlein *et al.* (2017) showed a differentiated adhesion behaviour between the bacterial strains *E. coli* and *S. aureus* on different types of steel LIPSS. It can be attributed to the variation in shape and size of rod-like *E. coli* and coccoid formed *S. aureus* as well as on the bacterial EPS production. It has already been shown that organisms that are smaller than the surface patterns exhibit a higher adhesion force due to the increased contact area (Whitehead and Verran 2006; Scardino *et al.* 2008). This trend was also observed in our study. In case of smaller grooves than bacteria size less adhering *S. aureus* were detected compared to bigger grooves. As shown in Figures 4 and 6, bacteria preferred to bind directly in the grooves between the periodic structures.

This *bacterial orientation* maximizes the contact area, which in turn leads to an increased adhesion and colonization of multiple micro-organisms (Hochbaum and Aizenberg 2010; Perera-Costa *et al.* 2014; Vasudevan

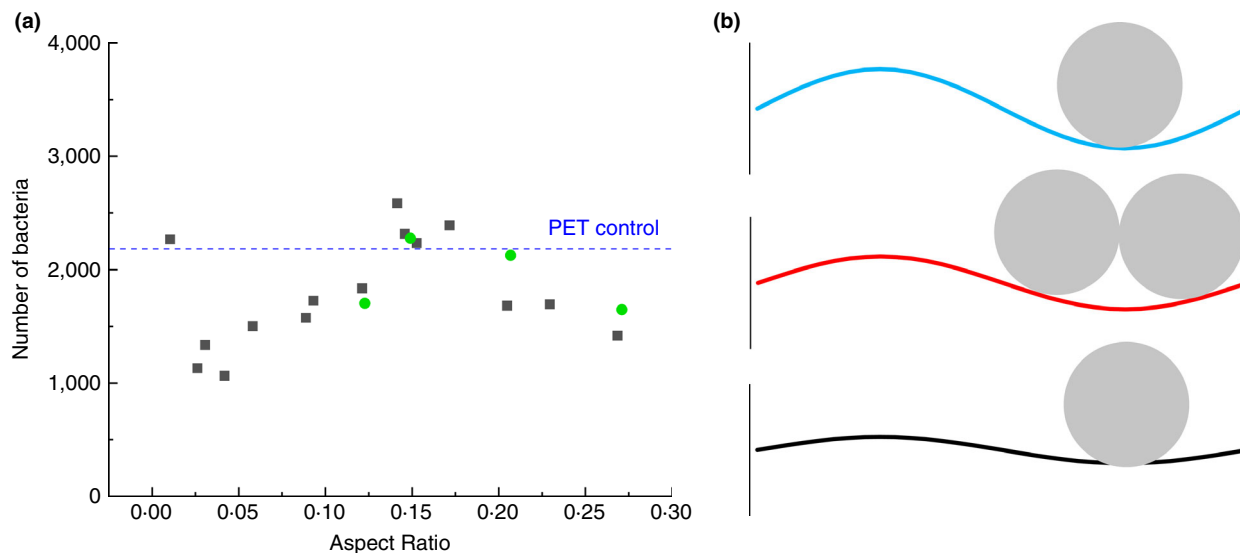


Figure 7 Schematic representation of the influence of the aspect ratio on the number of adhering bacteria for Ti and PET. (a) Number of *Staphylococcus aureus* according to the aspect ratio of the tested structures on PET and Ti specimens (■) PET and (●) Ti. (b) Scheme that illustrates the influence of different aspect ratio of 0.3, 0.2 and 0.1 on bacteria adhesion based on the finding on tested structures on PET and Ti specimens (—) 0.3; (—) 0.2 and (—) 0.1.

et al. 2014). It has been described previously that differently scaled topographies can reduce the biofilm formation and the adhesion of pathogens (Scardino *et al.* 2009; Scardino and de Nys 2011; Bixler and Bhushan 2012; Crawford *et al.* 2012; Hasan and Chatterjee 2015; Nir and Reches 2016; Elbourne *et al.* 2017). In this context, Majhi and Mishra (2020) demonstrated that laser patterning of surfaces represents an appropriate technology to reduce bacterial adhesion, since it affects the surface morphology as well as its wettability. Majhi and Mishra (2020) showed that the capability of *S. aureus* for the binding on a surface is dependent on the surface wettability and the average surface roughness which was tested with nanopillars with a size of 0.8 μm to 1.3 μm . According to Lam *et al.* (2016) sharp nanostructures are able to break the cell wall of pathogens and can kill them immediately. Anselme *et al.* (2010) investigated the interaction between bacteria and surface at a nanoscale and found that bacterial appendages (flagella, fimbriae etc.) determine the interaction with nanoscale patterns and thus influence bacterial adhesion. Puckett *et al.* (2010) compared in an *in vitro* study the adhesion of *S. aureus*, *S. epidermidis* and *Pseudomonas aeruginosa* on conventional nanosmooth to nanorough titanium produced by electron beam evaporation. A significant reduction for all tested bacteria strains was observed on structured titanium surfaces. Similar to our results Helbig *et al.* (2016) proved the inhibition of bacterial colonization by sub-cell sized DLIP topographies using *S. epidermidis* and *E. coli* irrespective of the surface chemistry. The results from our

study show that the mean roughness for periodic features of a surface is not the main influencing parameter for adhesion of bacteria (Supplementary Figure A3), but rather the aspect ratio of the DLIP structures determines bacterial adhesion preferences.

Depending on the separation distances between the structures, different adhesion interactions occur. While small separation distances (below 5 nm) mainly involve molecular interactions, macroscopic surface properties, such as surface free energy or hydrophobicity, are also important factors for the bacterial adhesion (Busscher and Weerkamp 1987; Cao *et al.* 2011). Increase of surface roughness within the macro, micro and nano scale enlarges the potential contact area, thereby creating a more effective and attractive adhesive surface for the bacteria (Preedy *et al.* 2014).

There are some limitations regarding this study. This study is limited to the investigated materials of PET and Ti, line-like periodic geometries and to only one bacteria strain. As other studies demonstrated previously, the adhesion and biofilm formation of laser-structured surfaces depend strongly on the type of microorganism tested on the respective surface (Lutey *et al.* 2018). We are aware of the limitation of our study that only one pathogen was tested on the structured surfaces. However, the most common species found in PJI is *Staphylococcus*. Therefore, we focused on *S. aureus* in this work (Arciola *et al.* 2005a; Arciola *et al.* 2005b). We are aware that a variety of other pathogens are associated with PJI, such as *P. aeruginosa*, *K. pneumonia* and *E. coli* (Peel *et al.* 2012). These

pathogens differ in size and shape (Young 2007) and therefore might exhibit another attachment profile compared to *S. aureus*. Further investigations using other pathogens are needed to assess the bacteria repellent effect of the structures in this manuscript in a broader range of PJI related bacteria. In addition, this study did not investigate the effect of the aspect ratio on a potential biofilm formation. However, we assume that the aspect ratio affects the adhesion behaviour of bacteria differently, if the bacteria are cultivated for a longer period due to the extracellular matrix secretion. Future work should consequently include longer cultivation times to investigate the influence of the aspect ratio on the biofilm formation. The structured Ti samples were limited to only four tested structures making it difficult to finally draw conclusions for influence of the tested patterns on the adhesion of bacteria. Future investigations will be needed to analyse a broader variety of structured Ti surfaces and their interaction with *S. aureus* as well as other common PJI pathogens. Furthermore, our findings regarding the various structures are limited with regard to the applied sterilization process that is different compared to the standard sterilization used by implant manufacturers. These differences might have an impact on the adhesion of bacteria. In addition, the reference sample was a polished TiAl6V4 disc, which represents a very common implant alloy. Future studies are envisaged to apply DLIP on TiAl6V4 alloy and UHMWPE as well as other relevant implant materials used for manufacturing of endoprosthesis.

This study showed that structuring on implant materials critically influences the adhesion and localization of *S. aureus* on the surface. We found that the aspect ratio was the main critical parameter for bacterial adhesion. A marked decrease of bacterial adhesion was observed for an aspect ratio range of 0.02 and 0.05. These findings will help to develop surface structures on implant materials that exhibit intrinsic bacteria repellent properties.

Acknowledgements

The authors acknowledge the excellent technical assistance of Carolin Schneider, Anja Schröder and Mandy Könnecke.

Conflict of Interest Statement

The authors certify that they have no affiliations with or involvement in any organization or entity with any financial interest (such as honoraria, educational grants or patent-licensing arrangements), or non-financial interest (such as personal or professional relationships, affiliations, knowledge or beliefs) in the subject matter or materials discussed in this manuscript.

Author's contribution

AKM: performed investigation, interpreted data, drafted the manuscript; MH: performed analyses, interpreted data, drafted the manuscript; CZ: helped with material preparation and sample production; MS: sample production, helped with writing the manuscript; AM: provided lab bacteria strain and microbiological expertise; TH: supervised the technical data, interpretation of data; AFL: developed study design, helped with writing the manuscript; JB: developed study design, interpretation of data, helped with writing the manuscript.

Disclaimer

This work was in part conducted within the context of the International Graduate School ABINEP and MEMORIAL at Otto von Guericke University (OVGU) Magdeburg, Germany, kindly supported by the European Structural and Investment Funds (ESF, 2014–2020) under the program “Sachsen-Anhalt WISSENSCHAFT Internationalisierung” (project no. ZS/2016/08/80645 and project no. ZS/2016/08/80646). This research and development project was also partially funded by the German Federal Ministry of Education and Research (BMBF) within the “Unternehmen Region, Innovation and structural transformation/WIR!” program, under contract number 03WIR2003B and implemented by the Project Management Agency Jülich (PTJ). M.S. acknowledges the Alexander von Humboldt Foundation. The authors are responsible for the content of this publication. The authors, their immediate families, and any research foundations with which they are affiliated have not received any financial payments or other benefits from any commercial entity related to the subject of this article.

References

- Anselme, K., Davidson, P., Popa, A.M., Giazzon, M., Liley, M. and Ploux, L. (2010) The interaction of cells and bacteria with surfaces structured at the nanometre scale. *Acta Biomater* **6**, 3824–3846.
- Arciola, C.R., An, Y.H., Campoccia, D., Donati, M.E. and Montanaro, L. (2005a) Etiology of implant orthopedic infections: a survey on 1027 clinical isolates. *Int J Artif Organs* **28**, 1091–1100.
- Arciola, C.R., Campoccia, D., Gamberini, S., Donati, M.E., Pirini, V., Visai, L., Speziale, P. and Montanaro, L. (2005b) Antibiotic resistance in exopolysaccharide-forming *Staphylococcus epidermidis* clinical isolates from orthopaedic implant infections. *Biomaterials* **26**, 6530–6535.
- Barrett, L. and Atkins, B. (2014) The clinical presentation of prosthetic joint infection. *J Antimicrob Chemother* **69**, i25–i27.

- Beach, W.R., Strecker, W.B., Coe, J., Manske, P.R., Schoenecker, P.L. and Dailey, L. (1991) Use of the Green transfer in treatment of patients with spastic cerebral palsy: 17-year experience. *J Pediatr Orthop* **11**, 731–736.
- Bhushan, B., Jung, Y.C. and Koch, K. (2009) Micro-, nano- and hierarchical structures for superhydrophobicity, self-cleaning and low adhesion. *Philos Trans A Math Phys Eng Sci* **367**, 1631–1672.
- Bixler, G.D. and Bhushan, B. (2012) Biofouling: lessons from nature. *Philos Trans A Math Phys Eng Sci* **370**, 2381–2417.
- Boháčová, M., Pazlarová, J., Fuchsová, V., Švehlákova, T. and Demnerová, K. (2019) Quantitative evaluation of biofilm extracellular DNA by fluorescence-based techniques. *Folia Microbiol* **64**, 567–577.
- Bonse, J., Höhm, S., Kirner, S.V., Rosenfeld, A. and Krüger, J. (2017) Laser-induced periodic surface structures – a scientific evergreen. *IEEE J Sel Top Quantum Electron* **23**, 1.
- Bremus-Koebberling, E.A., Beckemper, S., Koch, B. and Gillner, A. (2012) Nano structures via laser interference patterning for guided cell growth of neuronal cells. *J Laser Appl* **24**, 042013.
- Briandet, R., Herry, J.M. and Bellon-Fontaine, M.N. (2001) Determination of the van der Waals, electron donor and electron acceptor surface tension components of static Gram-positive microbial biofilms. *Colloids Surf B* **21**, 299–310.
- Bui, V.D., Mwangi, J.W., Meinshausen, A.-K., Mueller, A.J., Bertrand, J. and Schubert, A. (2020) Antibacterial coating of Ti-6Al-4V surfaces using silver nano-powder mixed electrical discharge machining. *Surf Coat Technol* **383**, 125254.
- Busscher, H.J. and Weerkamp, A.H. (1987) Specific and non-specific interactions in bacterial adhesion to solid substrata. *FEMS Microbiol Lett* **46**, 165–173.
- Cao, T., Tang, H., Liang, X., Wang, A., Auner, G.W., Salley, S.O. and Ng, K.Y. (2011) Nanoscale investigation on *E. coli* adhesion to modified silicone surfaces. *Methods Mol Biol* **736**, 379–388.
- Costerton, J.W., Stewart, P.S. and Greenberg, E.P. (1999) Bacterial biofilms: a common cause of persistent infections. *Science* **284**, 1318–1322.
- Crawford, R.J., Webb, H.K., Truong, V.K., Hasan, J. and Ivanova, E.P. (2012) Surface topographical factors influencing bacterial attachment. *Adv Colloid Interface Sci* **179–182**, 142–149.
- Cunha, A., Elie, A.-M., Plawinski, L., Serro, A.P., Botelho do Rego, A.M., Almeida, A., Urdaci, M.C., Durrieu, M.-C. and *et al.* (2016) Femtosecond laser surface texturing of titanium as a method to reduce the adhesion of *Staphylococcus aureus* and biofilm formation. *Appl Surf Sci* **360**, 485–493.
- Duarte, P.M., Reis, A.F., de Freitas, P.M. and Ota-Tsuzuki, C. (2009) Bacterial adhesion on smooth and rough titanium surfaces after treatment with different instruments. *J Periodontol* **80**, 1824–1832.
- Elbourne, A., Crawford, R.J. and Ivanova, E.P. (2017) Nano-structured antimicrobial surfaces: from nature to synthetic analogues. *J Colloid Interface Sci* **508**, 603–616.
- Epperlein, N., Menzel, F., Schwibbert, K., Koter, R., Bonse, J., Sameith, J., Krüger, J. and Toepel, J. (2017) Influence of femtosecond laser produced nanostructures on biofilm growth on steel. *Appl Surf Sci* **418**, 420–424.
- Eposito, M., Murray-Curtis, L., Grusovin, M.G., Coulthard, P. and Worthington, H.V. (2007) Interventions for replacing missing teeth: different types of dental implants. *Cochrane Database Syst Rev* **4**, Cd003815.
- Fehring, T.K., Odum, S., Calton, T.F. and Mason, J.B. (2000) Articulating versus static spacers in revision total knee arthroplasty for sepsis. *Orthop Rel Res* **380**, 9–16.
- Fehring, T.K., Odum, S., Calton, T.F. and Mason, J.B. (2000) Articulating versus static spacers in revision total knee arthroplasty for sepsis. The Ranawat Award. *Clin Orthop Relat Res* **380**, 9–16.
- Fisher, J. and Dowson, D. (1991) Tribology of total artificial joints. *Proc Inst Mech Eng H* **205**, 73–79.
- Flemming, H.-C. and Wingender, J. (2010) The biofilm matrix. *Nat Rev Microbiol* **8**, 623–633.
- Florian, C., Kirner, S.V., Krüger, J. and Bonse, J. (2020) Surface functionalization by laser-induced periodic surface structures. *J Laser Appl* **32**, 022063.
- Fu, Y., Soldara, M., Wang, W., Voisiat, B. and Lasagni, A.F. (2019) Picosecond laser interference patterning of periodical micro-architectures on metallic molds for hot embossing. *Materials* **12**, 3409.
- Gao, K., Chen, S., Wang, L., Zhang, W., Kang, Y., Dong, Q., Zhou, H. and Li, L. (2010) Anterior cruciate ligament reconstruction with LARS artificial ligament: a multicenter study with 3- to 5-year follow-up. *Arthroscopy* **26**, 515–523.
- Gibon, E., Amanatullah, D.F., Loi, F., Pajarinen, J., Nabeshima, A., Yao, Z., Hamadouche, M. and Goodman, S.B. (2017) The biological response to orthopaedic implants for joint replacement: part I: Metals. *J Biomed Mater Res B Appl Biomater* **105**, 2162–2173.
- Goldberg, A.L., Kettelhut, I.C., Furuno, K., Fagan, J.M. and Baracos, V. (1988) Activation of protein breakdown and prostaglandin E2 production in rat skeletal muscle in fever is signaled by a macrophage product distinct from interleukin 1 or other known monokines. *J Clin Invest* **81**, 1378–1383.
- Guo, Z., Liu, W. and Su, B.L. (2011) Superhydrophobic surfaces: from natural to biomimetic to functional. *J Colloid Interface Sci* **353**, 335–355.
- Hall-Stoodley, L., Costerton, J.W. and Stoodley, P. (2004) Bacterial biofilms: from the natural environment to infectious diseases. *Nat Rev Microbiol* **2**, 95–108.
- Hasan, J. and Chatterjee, K. (2015) Recent advances in engineering topography mediated antibacterial surfaces. *Nanoscale* **7**, 15568–15575.
- Hasan, J., Crawford, R.J. and Ivanova, E.P. (2013) Antibacterial surfaces: the quest for a new generation of biomaterials. *Trends Biotechnol* **31**, 295–304.

- Helbig, R., Günther, D., Friedrichs, J., Rößler, F., Lasagni, A. and Werner, C. (2016) The impact of structure dimensions on initial bacterial adhesion. *Biomater Sci* **4**, 1074–1078.
- Hochbaum, A.I. and Aizenberg, J. (2010) Bacteria pattern spontaneously on periodic nanostructure arrays. *Nano Lett* **10**, 3717–3721.
- Höhm, S., Rosenfeld, A., Krüger, J. and Bonse, J. (2015) Laser-induced periodic surface structures on titanium upon single- and two-color femtosecond double-pulse irradiation. *Opt Express* **23**, 25959–25971.
- Højby, N., Bjarsholt, T., Givskov, M., Molin, S. and Ciofu, O. (2010) Antibiotic resistance of bacterial biofilms. *Int J Antimicrob Agents* **35**, 322–332.
- Højby, N., Bjarsholt, T., Moser, C., Bassi, G.L., Coenye, T., Donelli, G., Hall-Stoodley, L., Holá, V. *et al.* (2015) ESCMID guideline for the diagnosis and treatment of biofilm infections 2014. *Clin Microbiol Infect* **21**(Suppl 1), S1–25.
- Inđrišūnas, S., Voisiat, B., Gedvilas, M. and Račiukaitis, G. (2017) New opportunities for custom-shape patterning using polarization control in confocal laser beam interference setup. *J Laser Appl* **29**, 011501.
- Ivanova, E.P., Truong, V.K., Wang, J.Y., Berndt, C.C., Jones, R.T., Yusuf, I.I., Peake, I., Schmidt, H.W. *et al.* (2010) Impact of nanoscale roughness of titanium thin film surfaces on bacterial retention. *Langmuir* **26**, 1973–1982.
- Jaggessar, A., Shahali, H., Mathew, A. and Yarlagadda, P.K.D.V. (2017) Bio-mimicking nano and micro-structured surface fabrication for antibacterial properties in medical implants. *J Nanobiotechnol* **15**, 64.
- Jalil, S.A., Akram, M., Bhat, J.A., Hayes, J.J., Singh, S.C., ElKabbash, M. and Guo, C. (2020) Creating superhydrophobic and antibacterial surfaces on gold by femtosecond laser pulses. *Appl Surf Sci* **506**, 144952.
- Kvist, J., Ek, A., Sporrstedt, K. and Good, L. (2005) Fear of re-injury: a hindrance for returning to sports after anterior cruciate ligament reconstruction. *Knee Surg Sports Traumatol Arthrosc* **13**, 393–397.
- Lam, S.J., O'Brien-Simpson, N.M., Pantarat, N., Sulistio, A., Wong, E.H.H., Chen, Y.-Y., Lenzo, J.C., Holden, J.A. *et al.* (2016) Combating multidrug-resistant Gram-negative bacteria with structurally nanoengineered antimicrobial peptide polymers. *Nat Microbiol* **1**, 16162.
- Lang, V., Rank, A. and Lasagni, A.F. (2017) Large area one-step fabrication of three-level multiple-scaled micro and nanostructured nickel sleeves for roll-to-roll hot embossing. *Adv Eng Mater* **19**, 1700126.
- Lang, V., Roch, T. and Lasagni, A. (2016) *World Record in High Speed Laser Surface Microstructuring of Polymer and Steel Using Direct Laser Interference Patterning*. SPIE. <https://doi.org/10.1117/12.2216203>
- Lasagni, A., Acevedo, D., Cornejo, M., Lasagni, F., Politano, M., Barbero, C. and Mücklich, F. (2009) *Direct Fabrication of Surface Architectures on Polymers and Copolymers Using Laser Interference Patterning*. SPIE. <https://doi.org/10.1117/12.821090>
- Lentino, J.R. (2003) Prosthetic joint infections: bane of orthopedists, challenge for infectious disease specialists. *Clin Infect* **36**, 1157–1161.
- Lüdecke, C., Bossert, J., Roth, M. and Jandt, K.D. (2013) Physical vapor deposited titanium thin films for biomedical applications: reproducibility of nanoscale surface roughness and microbial adhesion properties. *Appl Surf Sci* **280**, 578–589.
- Lunelli, L., Potrich, C., Pasquardini, L. and Pederzoli, C. (2012) Nanostructured functionalized surfaces. In *Encyclopedia of nanotechnology* ed. Bhushan, B. pp. 1760–1766. Dordrecht: Springer, Netherlands.
- Lutey Adrian H. A., Gemini Laura, Romoli Luca, Lazzini Gianmarco, Fuso Francesco, Faucon Marc, Kling Rainer (2018) Towards Laser-Textured Antibacterial Surfaces. *Scientific Reports*, **8** (1), <http://dx.doi.org/10.1038/s41598-018-28454-2>.
- Majhi, S. and Mishra, A. (2020) Modulating surface energy and surface roughness for inhibiting microbial growth. In *Engineered antimicrobial surfaces* eds. Snigdha, S., Thomas, S., Radhakrishnan, E.K. and Kalarikkal, N., pp. 109–121. Singapore: Springer Singapore.
- Marculescu, C.E. and Cantey, J.R. (2008) Polymicrobial prosthetic joint infections: risk factors and outcome. *Clin Orthop Relat Res* **466**, 1397.
- Mauerhan, D.R., Nelson, C.L., Smith, D.L., Fitzgerald, R.H. Jr, Slama, T.G., Petty, R.W., Jones, R.E. and Evans, R.P. (1994) Prophylaxis against infection in total joint arthroplasty. One day of cefuroxime compared with three days of cefazolin. *J Bone Joint Surg Am* **76**, 39–45.
- Medilanski, E., Kaufmann, K., Wick, L.Y., Wanner, O. and Harms, H. (2002) Influence of the surface topography of stainless steel on bacterial adhesion. *Biofouling* **18**, 193–203.
- Meehan, J., Jamali, A.A. and Nguyen, H. (2009) Prophylactic antibiotics in hip and knee arthroplasty. *J Bone Joint Surg Am* **91**, 2480–2490.
- Melvin, A., Litsky, A., Mayerson, J., Witte, D., Melvin, D. and Juncosa-Melvin, N. (2010) An artificial tendon with durable muscle interface. *J Orthop Res* **28**, 218–224.
- Morgan, T.D. and Wilson, M. (2001) The effects of surface roughness and type of denture acrylic on biofilm formation by *Streptococcus oralis* in a constant depth film fermentor. *J Appl Microbiol* **91**, 47–53.
- Nair, P.K., Bhat, V.G. and Vaz, M.S. (2014) Prosthetic joint infections—a clinico-microbiological perspective: Review article. *World J Clin Infect Dis* **4**, 9–15. <https://doi.org/10.5495/wjcid.v4.i3.9>
- Nir, S. and Reches, M. (2016) Bio-inspired antifouling approaches: the quest towards non-toxic and non-biocidal materials. *Curr Opin Biotechnol* **39**, 48–55.
- Nyvad, B. and Fejerskov, O. (1987) Scanning electron microscopy of early microbial colonization of human

- enamel and root surfaces in vivo. *Scand J Dent Res* **95**, 287–296.
- Oliveira, V., Polushkin, N.I., Conde, O. and Vilar, R. (2012) Laser surface patterning using a Michelson interferometer and femtosecond laser radiation. *Opt Laser Technol* **44**, 2072–2075.
- Otto, M. (2008) Staphylococcal biofilms. *Curr Top Microbiol Immunol* **322**, 207–228.
- Pavel, A., Smith, R.L., Ballard, A. and Larsen, I.J. (1974) Prophylactic antibiotics in clean orthopaedic surgery. *J Bone Joint Surg Am* **56**, 777–782.
- Pavithra, D. and Doble, M. (2008) Biofilm formation, bacterial adhesion and host response on polymeric implants—issues and prevention. *Biomed Mater* **3**, 034003.
- Peel, T.N., Cheng, A.C., Buising, K.L. and Choong, P.F. (2012a) Microbiological aetiology, epidemiology, and clinical profile of prosthetic joint infections: are current antibiotic prophylaxis guidelines effective? *Antimicrob Agents Chemother* **56**, 2386–2391.
- Perera-Costa, D., Bruque, J.M., González-Martín, M.L., Gómez-García, A.C. and Vadillo-Rodríguez, V. (2014) Studying the influence of surface topography on bacterial adhesion using spatially organized microtopographic surface patterns. *Langmuir* **30**, 4633–4641.
- Piper, K.E., Jacobson, M.J., Cofield, R.H., Sperling, J.W., Sanchez-Sotelo, J., Osmon, D.R., McDowell, A., Patrick, S. *et al.* (2009) Microbiologic diagnosis of prosthetic shoulder infection by use of implant sonication. *J Clin Microbiol* **47**, 1878–1884.
- Pollard, J.P., Hughes, S.P., Scott, J.E., Evans, M.J. and Benson, M.K. (1979) Antibiotic prophylaxis in total hip replacement. *BMJ* **1**, 707–709.
- Preedy, E., Perni, S., Nipič, D., Bohinc, K. and Prokopovich, P. (2014) Surface roughness mediated adhesion forces between borosilicate glass and gram-positive bacteria. *Langmuir* **30**, 9466–9476.
- Puckett, S.D., Taylor, E., Raimondo, T. and Webster, T.J. (2010) The relationship between the nanostructure of titanium surfaces and bacterial attachment. *Biomaterials* **31**, 706–713.
- Qazi, S.N., Counil, E., Morrissey, J., Rees, C.E., Cockayne, A., Winzer, K., Chan, W.C., Williams, P. *et al.* (2001) agr expression precedes escape of internalized *Staphylococcus aureus* from the host endosome. *Infect Immun* **69**, 7074–7082.
- Rank, A., Lang, V. and Lasagni, A.F. (2017) High-speed roll-to-roll hot embossing of micrometer and sub micrometer structures using seamless direct laser interference patterning treated sleeves. *Adv Eng Mater* **19**, 1700201.
- Renner, L.D. and Weibel, D.B. (2011) Physicochemical regulation of biofilm formation. *MRS Bull* **36**, 347–355.
- Rodriguez, A., Echeverría, M., Ellman, M., Perez, N., Verevkin, Y.K., Peng, C.S., Berthou, T., Wang, Z. *et al.* (2009) Laser interference lithography for nanoscale structuring of materials: from laboratory to industry. *Microelectron Eng* **86**, 937–940.
- Römer, G.R.B.E., Huis in't Veld, A.J., Meijer, J. and Groenendijk, M.N.W. (2009) On the formation of laser induced self-organizing nanostructures. *CIRP Ann* **58**, 201–204.
- Rosenkranz, A., Hans, M., Gachot, C., Thome, A., Bonk, S. and Mücklich, F. (2016) Laser interference patterning – tailoring of contact area for frictional and antibacterial properties. *Lubricants* **4**, 2.
- Scardino, A.J., Guenther, J. and de Nys, R. (2008) Attachment point theory revisited: the fouling response to a microtextured matrix. *Biofouling* **24**, 45–53.
- Scardino, A.J., Hudleston, D., Peng, Z., Paul, N.A. and de Nys, R. (2009) Biomimetic characterisation of key surface parameters for the development of fouling resistant materials. *Biofouling* **25**, 83–93.
- Scardino, A.J. and de Nys, R. (2011) Mini review: biomimetic models and bioinspired surfaces for fouling control. *Biofouling* **27**, 73–86.
- Schwibbert, K., Menzel, F., Epperlein, N., Bonse, J. and Krüger, J. (2019) Bacterial adhesion on femtosecond laser-modified polyethylene. *Materials* **12**, 3107.
- Singh, A.V., Galluzzi, M., Borghi, F., Indrieri, M., Vyas, V., Podestà, A. and Gade, W.N. (2013) Interaction of bacterial cells with cluster-assembled nanostructured Titania surfaces: an atomic force microscopy study. *J Nanosci Nanotechnol* **13**, 77–85.
- Singh, A.V., Vyas, V., Patil, R., Sharma, V., Scopelliti, P.E., Bongiorno, G., Podestà, A., Lenardi, C. *et al.* (2011) Quantitative characterization of the influence of the nanoscale morphology of nanostructured surfaces on bacterial adhesion and biofilm formation. *PLoS ONE* **6**, e25029.
- Smucny, M., Menendez, M.E., Ring, D., Feeley, B.T. and Zhang, A.L. (2015) Inpatient surgical site infection after shoulder arthroplasty. *J Shoulder Elbow Surg* **24**, 747–753.
- Soldera, M., Wang, Q., Soldera, F., Lang, V., Abate, A. and Lasagni, A.F. (2020) Toward high-throughput texturing of polymer foils for enhanced light trapping in flexible perovskite solar cells using roll-to-roll hot embossing. *Adv Eng Mater* **22**, 1901217.
- Sousa, A., Carvalho, A., Pereira, C., Reis, E., Santos, A.C., Abreu, M., Soares, D., Fragoso, R. *et al.* (2018) Economic impact of prosthetic joint infection – an evaluation within the Portuguese National Health System. *J Bone Joint Infect* **3**, 197–202.
- Sutula, L.C., Collier, J.P., Saum, K.A., Currier, B.H., Currier, J.H., Sanford, W.M., Mayor, M.B., Wooding, R.E. *et al.* (1995) The Otto Aufranc Award. Impact of gamma sterilization on clinical performance of polyethylene in the hip. *Clin Orthop Relat Res* **319**, 28–40.
- Tande, A.J. and Patel, R. (2014) Prosthetic joint infection. *Clin Microbiol Rev* **27**, 302–345.
- Truong, V.K., Lapovok, R., Estrin, Y.S., Rundell, S., Wang, J.Y., Fluke, C.J., Crawford, R.J. and Ivanova, E.P. (2010) The influence of nano-scale surface roughness on bacterial

- adhesion to ultrafine-grained titanium. *Biomaterials* **31**, 3674–3683.
- Ulrich, S.D., Seyler, T.M., Bennett, D., Delanois, R.E., Saleh, K.J., Thongtrangan, I., Kuskowski, M., Cheng, E.Y. *et al.* (2008) Total hip arthroplasties: what are the reasons for revision? *Int Orthop* **32**, 597–604.
- Vasudevan, R., Kennedy, A.J., Merritt, M., Crocker, F.H. and Baney, R.H. (2014) Microscale patterned surfaces reduce bacterial fouling-microscopic and theoretical analysis. *Colloids Surf B Biointerfaces* **117**, 225–232.
- Vincenc Obona, J., Ocelík, V., Skolski, J.Z.P., Mitko, V.S., Römer, G.R.B.E., Huis in't Veld, A.J. and De Hosson, J.T.M. (2011) On the surface topography of ultrashort laser pulse treated steel surfaces. *Appl Surf Sci* **258**, 1555–1560.
- Voisiat, B., Wang, W., Holzhey, M. and Lasagni, A.F. (2019) Improving the homogeneity of diffraction based colours by fabricating periodic patterns with gradient spatial period using Direct Laser Interference Patterning. *Sci Rep* **9**, 7801.
- Webb, J.S., Givskov, M. and Kjelleberg, S. (2003) Bacterial biofilms: prokaryotic adventures in multicellularity. *Curr Opin Microbiol* **6**, 578–585.
- Wetters, N.G., Murray, T.G., Moric, M., Sporer, S.M., Paprosky, W.G. and Della Valle, C.J. (2013) Risk factors for dislocation after revision total hip arthroplasty. *Clin Orthop Relat Res* **471**, 410–416.
- Whitehead, K.A., Colligon, J. and Verran, J. (2005) Retention of microbial cells in substratum surface features of micrometer and sub-micrometer dimensions. *Colloids Surf B Biointerfaces* **41**, 129–138.
- Whitehead, K.A. and Verran, J. (2006) The effect of surface topography on the retention of microorganisms. *Food Bioprod Process* **84**, 253–259.
- Whitehead, K.A. and Verran, J. (2007) The effect of surface properties and application method on the retention of *Pseudomonas aeruginosa* on uncoated and titanium-coated stainless steel. *Int Biodeterior Biodegradation* **60**, 74–80.
- Wu, N., Wang, Z., Wang, X., Shimotsuna, Y., Nishi, M., Miura, K. and Hirao, K. (2011a) Nano-periodic structure formation on titanium thin film with a Femtosecond laser. *J Ceram Soc Jpn* **119**, 898–901.
- Wu, Y., Zitelli, J.P., TenHuisen, K.S., Yu, X. and Libera, M.R. (2011b) Differential response of Staphylococci and osteoblasts to varying titanium surface roughness. *Biomaterials* **32**, 951–960.
- Young, K.D. (2007) Bacterial morphology: why have different shapes? *Curr Opin Microbiol* **10**, 596–600.
- Zimmerli, A.T.A.W. (2008) Diagnosis and treatment of implant-associated septic arthritis and osteomyelitis. *Curr Infect Dis Rep* **10**, 394–403.
- Zimmerli, W. and Sendi, P. (2011) Pathogenesis of implant-associated infection: the role of the host. *Semin Immunopathol* **33**, 295–306.
- Zwahr, C., Helbig, R., Werner, C. and Lasagni, A.F. (2019a) Fabrication of multifunctional titanium surfaces by producing hierarchical surface patterns using laser based ablation methods. *Sci Rep* **9**, 6721.
- Zwahr, C., Welle, A., Weingärtner, T., Heinemann, C., Kruppke, B., Gulow, N., Holthaus, M.G. and Fabián Lasagni, A. (2019b) Ultrashort pulsed laser surface patterning of titanium to improve osseointegration of dental implants. *Adv Eng Mater* **21**, 1900639.

Supporting Information

Additional Supporting Information may be found in the online version of this article:

Figure A1 Schematic illustration of the (a) DLIP principle based on two overlapping coherent beams at the sample surface that generate and interference pattern. (b) Schematics of the roll-to-roll hot embossing method

Figure A2 SEM images of a (a) DLIP-treated Ti surface and a (b) hot embossed PET sample from a DLIP-structured Ni mould.

Figure A3 Number of adhering *S. aureus* bacteria according to the arithmetic mean roughness (R_a) for PET and Ti structures.

Appendix S1 Description of the DLIP principle and the roll-to-roll (R2) hot embossing system.